SCIENTIFIC REPORTS

OPEN

SUBJECT AREAS:
ELECTRONIC PROPERTIES AND MATERIALS
CHARACTERIZATION AND ANALYTICAL TECHNIQUES
ELECTRONIC STRUCTURE
MAGNETIC PROPERTIES AND MATERIALS

Received
29 August 2013

Accepted
17 December 2013

Published
14 January 2014

Correspondence and requests for materials should be addressed to H.-J.N. (ffnhj@chonnam.ac.kr)

* Current address: Center for Correlated Electron Systems, Institute for Basic Science (IBS), Seoul 151-747, Korea.

# Direct Observation of Localized Spin Antiferromagnetic Transition in $PdCrO_2$ by Angle-Resolved Photoemission Spectroscopy

Han-Jin Noh[1], Jinwon Jeong[1], Bin Chang[1], Dahee Jeong[1], Hyun Sook Moon[1], En-Jin Cho[1], Jong Mok Ok[2], Jun Sung Kim[2], Kyoo Kim[2], B. I. Min[2], Han-Koo Lee[3], Jae-Young Kim[3], Byeong-Gyu Park[3], Hyeong-Do Kim[3]* & Seongsu Lee[4]

[1]Department of Physics, Chonnam National University, Gwangju 500-757, Korea, [2]Department of Physics, Pohang University of Science and Technology, Pohang 790-784, Korea, [3]Pohang Accelerator Laboratory, Pohang University of Science and Technology, Pohang 790-784, Korea, [4]Korea Atomic Energy Research Institute, Daejeon, 305-353, Korea.

**We report the first case of the successful measurements of a localized spin antiferromagnetic transition in delafossite-type $PdCrO_2$ by angle-resolved photoemission spectroscopy (ARPES). This demonstrates how to circumvent the shortcomings of ARPES for investigation of magnetism involved with localized spins in limited size of two-dimensional crystals or multi-layer thin films that neutron scattering can hardly study due to lack of bulk compared to surface. Also, our observations give direct evidence for the spin ordering pattern of $Cr^{3+}$ ions in $PdCrO_2$ suggested by neutron diffraction and quantum oscillation measurements, and provide a strong constraint that has to be satisfied by a microscopic mechanism for the unconventional anomalous Hall effect recently reported in this system.**

Angle-resolved photoemission spectroscopy (ARPES) has been one of the most powerful tools to investigate the electronic structure of crystalline solids. With the help of the third generation synchrotron facilities and the electron spectrometers with angle resolved mode, ARPES now can be utilized for the study of the magnetic structure as well as the electronic one[1]. In particular, ARPES has revealed various kinds of magnetic fluctuations in high-temperature superconductors and magnetic thin films, providing key information to understand the underlying physics[2,3]. However, there is the last piece of the puzzle left in ARPES for magnetic structure study: observing a long range ordering of localized magnetic moments. Actually, Fermi surface (FS) folding induced by many kinds of order other than localized magnetic moments has been observed by ARPES. The most probable reason for this exception is that the potential difference by localized moment ordering is so small that the band electrons can hardly feel the potential change, resulting in negligible or non-detectable changes in the photoemission signals. Here, at long last, we report the first case of the successful ARPES measurements of a localized spin antiferromagnetic transition in delafossite-type $PdCrO_2$. Our observations give direct evidence for the spin ordering pattern of $Cr^{3+}$ ions in $PdCrO_2$ suggested by neutron diffraction[4,5] and quantum oscillation measurements[6], and provide a strong constraint that has to be satisfied by a microscopic mechanism for the unconventional anomalous Hall effect (UHAE) recently reported in this system[7]. Also, this demonstrates a new pathway for investigation of magnetism in limited size of two-dimensional crystals or multi-layer thin films that neutron scattering can hardly study due to lack of bulk compared to surface.

## Results

Metallic delafossite-type oxides (Fig. 1a) $ABO_2$ (A = Pd and Pt; B = Cr, Co, and Rh) are famous for their good conductivity[8]. In particular, the $PdCoO_2$ exhibits the best conductivity in the normal state oxides. The conductivity is even better than that of Pd metal, and so this case has been scrutinized at length by ARPES study[9], x-ray absorption spectroscopy study[10], *ab-initio* band structure calculations[11,12], and thermo-transport study[13]. The large two-dimensional FS consisting of the fast conduction electrons with a long life time was confirmed to be the origin of the anisotropic high conductivity in the previous studies. The interesting and noticeable features for

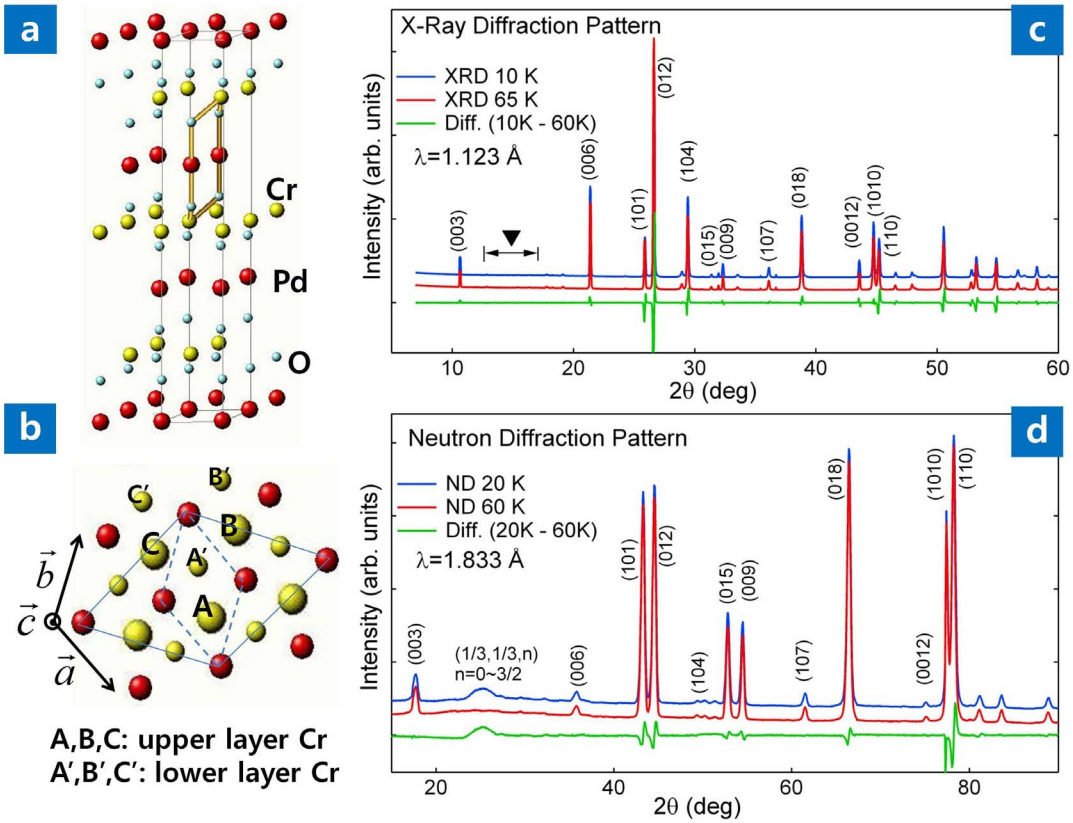


**Figure 1 | Crystal structure and corresponding diffraction patterns.** (a), Crystal structure of delafossite-type $PdCrO_2$ (space group $R\bar{3}m$) with the conventional hexagonal unit cell. Each Pd (red sphere) layer and Cr (yellow sphere) layer forms a triangular lattice. The yellow rods between Cr, O, and Pd atoms denote the shortest path from a Pd layer to a Cr layer. (b), Top view along the c-axis. For convenience, the O atoms are not displayed. When the Cr layers have the 120° antiferromagnetic ordering, there are three kinds of Cr atoms with respect to the spin directions, denoted as A(A'), B(B'), and C(C'), in the adjacent upper(lower) layer. The small rhombus drawn with the dotted lines represents the paramagnetic unit cell, while the large rhombus with the solid lines represents the $\sqrt{3} \times \sqrt{3}$ super-structured antiferromagnetic unit cell. (c), X-ray diffraction patterns for the powder samples obtained at the temperature above and below $T_N = 37.5$ K. The difference curve (green line) indicates that there is no structure transition across the magnetic transition. (d), Neutron diffraction patterns obtained above and below $T_N$. The broad hump around $2\theta = 26°$ in the blue curve is a bunch of superstructure peaks corresponding to (1/3 1/3 n) (n = 0, 1/2, 1, 3/2).

$PdCoO_2$ are two-fold; the metallic Pd layers with the large *sp*-like band dispersions and the insulating triangular lattice $CoO_2$ with the low-spin (S = 0, $3d^6$) configuration. When the $Co^{3+}$ ion in the trigonally distorted octahedron $MO_6$ (M = transition metal ion) is replaced by $Cr^{3+}$ ions in the same crystal structure, the only difference with respect to the electronic structure lies in the spin quantum number of the $t_{2g}$ manifolds in the transition-metal ions. It simply changes the quantum number from S = 0 (full filling) to S = 3/2 (half filling), i.e. from non-magnetic $CoO_2$ to magnetic $CrO_2$ triangular lattice. In this case, since the Cr ions form a two-dimensional triangular lattice (2DTL) with the antiferromagnetically interacting local spins, the system becomes much more attractive. As is well known, this kind of spin geometry would produce the magnetic frustration and the possible quantum liquid ground state[14,15]. Further, this system has highly metallic layers, and so it provides a rare opportunity to investigate the interactions between the frustrated local magnetic moments in a 2DTL and the itinerant electrons in an adjacent layer. Indeed, recent transport studies have reported that an unconventional anomalous Hall effect (UAHE) was observed in this system, revealing an exotic behavior of an antiferromagnetic 2DTL with metallic layers[6,7]. However, since the UAHE reported in this system requires an incompatible spin ordering to the known antiferromagnetic ordering, more refined experimental and theoretical characterization is essential to understand the underlying physics.

Figure 1b shows a top view of an upper Cr (big yellow balls) layer, a Pd (red balls) layer, and a lower Cr (small yellow balls) layer in the delafossite structure. When the system is antiferromagnetic below $T_N$ = 37.5 K, the neutron powder diffraction study suggested that the spin directions of the Cr ions are ordered into a non-collinear 120° structure. In this spin structure, the Cr ions are classified into three kinds (denoted as A, B, and C in Fig. 1b) with respect to their spin directions. The intensity analysis of the magnetic Bragg peaks suggested that the three spin vectors lie in a plane containing the c-axis[4,5]. The adjacent Cr layer has the same structure as denoted as A', B', and C' in Fig. 1b, but the exact phase difference between the layers is not clear. The crystal structure and the suggested magnetic phase for our samples were checked by the X-ray diffraction (XRD) and neutron diffraction (ND) measurements above and below $T_N$ as shown in Figs. 1(c) and 1(d). The superstructure peaks around 26° in the low temperature (T = 20 K) ND pattern are not seen at the paramagnetic phase (T = 60 K), indicating that the origin of the peaks is spin ordering. Meanwhile, there are neither superstructure peaks at the corresponding angles (▼) nor differences between the XRD patterns above and below $T_N$ except for the normal peak position shifts due to thermal lattice expansion. This shows that the symmetry of the crystal structure does not change across the magnetic transition.

The S = 3/2 spin quantum number of the $Cr^{3+}$ ions and the metallic behavior of the Pd layers are revealed in the Cr $2p \rightarrow 3d$ x-ray absorption spectra (XAS) and the Pd 3*d* x-ray photoemission

spectrum (XPS) as shown in Fig. 2. The XAS spectra drawn with red line (T = 60 K) and with blue line (T = 28 K) in Fig. 2a were obtained with the photon polarization vector normal to the *ab*-plane of the single crystalline samples. The electron configuration and the spin state can be determined by comparing the XAS spectrum with that of a reference system since a transition metal $2p \rightarrow 3d$ absorption spectrum is a kind of fingerprint for the electronic energy structure of the transition metal ions[16]. If we compare our XAS spectra with that of $Cr_2O_3$ and of $CrO_2$, each of which represents a trivalent S = 3/2 Cr ion and a tetravalent S = 1 Cr ion, respectively[17], the valence and the spin state of the Cr ions in $PdCrO_2$ are clearly determined to be trivalent and S = 3/2 irrespective of the magnetic phase. The metallic Pd layers can be checked by analyzing the Pd 3*d* XPS spectrum as shown in Fig. 2b. As is the case of iso-structural $PdCoO_2$, the asymmetric line shape is prominent, indicating that the photoholes are well screened by the conduction electrons through the creation of electron-hole pairs across the Fermi level[9]. The quantitative line shape analysis with the Doniach-Šunjić (DS) model[18] gave the asymmetric parameter value of $\alpha = 0.26$. This value is a little larger than that of Pd metal but equal to that of $PdCoO_2$, and lies in a reasonable region[9,19]. These spectroscopic observations support the idea that $PdCrO_2$ is an ideal system to investigate the detailed balance between the itinerant electrons and the adjacent localized spins in the 2DTL.

A phase transition involving the $\sqrt{3} \times \sqrt{3}\,R30^\circ$ superstructure was directly observed by our ARPES measurements as shown in Fig. 3a. At the temperature of 100 K (bottom), we observed only one large electron-like hexagonal FS in a Brillouin zone (BZ). Meanwhile, at $T$ = 20 K (top), it is clearly seen that the extra FS features other than the original FS appear in our constant energy ARPES intensity map at the Fermi level ($E_F$). Since $PdCrO_2$ is known to have an antiferromagnetic phase below $T_N = 37.5$ K, these new FSs are naturally attributed to the folded FS's arising from the reduced BZ of an antiferromagnetic phase. If this is the case, it is a milestone in ARPES because no ARPES study has reported a successful observation on a long range ordering of localized spins in a magnetic system. However, to justify this conclusion, the other possible reasons must be checked. First, a structural transition accompanied by the antiferromagnetic transition is suspected, but this possibility can be excluded by our temperature-dependent ND/XRD as explained in Figs. 1(c) and 1(d). The temperature-dependent diffractions show only a normal thermal expansion behavior and no abrupt peak shift around $T_N$. Second, charge ordering or charge density wave is a candidate, but this can be also ruled out by the temperature-dependent X-ray diffraction study that shows no extra-peaks below $T_N$. Furthermore, we did not observe any signal indicating mixed valency of the cations or charge disproportionation in our temperature-dependent core-level XPS study, as partly shown in Fig. 2. Last, a temperature-dependent surface reconstruction should be checked for a possible origin since ARPES is a surface-sensitive probe. As to this possibility, however, a recent ARPES study on $PdCrO_2$ has reported totally different and temperature-independent surface FSs from ours as well as almost identical bulk FSs to ours[20]. This clearly shows that our temperature-dependent FS folding is not relevant to a surface reconstruction. Thus, the band folding in our ARPES data cannot but be relevant to the magnetic transition.

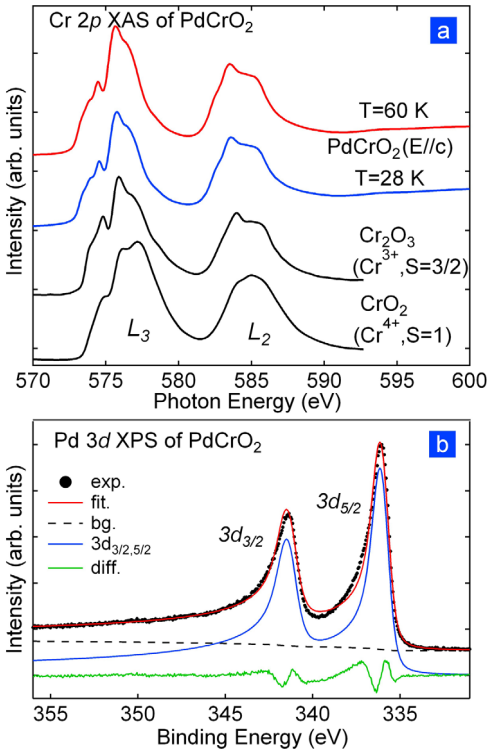


**Figure 2 | X-ray absorption/photoemission spectra.** (a), Cr 2p X-ray absorption spectra of $PdCrO_2$, $Cr_2O_3$, and $CrO_2$. The first three spectra look very similar while the fourth one looks quite different from the others. The similarity in transition metal $2p \rightarrow 3d$ XAS indicates that the electron configuration of the ions is the same. The two reference spectra are taken from the literature[17]. (b), Pd 3*d* X-ray photoemission spectrum of $PdCrO_2$. The blue solid line is the simulated spectrum based on the DS line shape model. The red solid line, black dotted line, and the green solid line are the fitting spectrum, the background, and the fitting error, respectively.

The electronic structure of $PdCrO_2$ measured by ARPES in the paramagnetic phase is very similar to that of iso-structural non-magnetic $PdCoO_2$ except for the absence of surface states[9,12]. Both systems commonly have a two-dimensional FS with a rounded hexagonal cross section in a BZ. In Fig. 3b, we show the ARPES image cut along the vertical dotted line in Fig. 3a bottom and the calculated band structure along the Γ-K line using the linearized augmented plane wave method with local orbitals (LAPW + LO) in the generalized gradient approximation (GGA). For simplicity, the calculation was set in the rhombohedral unit cell assuming a ferromagnetic ordering, which produces the over-split Fermi points, $P_1$ and $P_2$. Except for the spin-split feature, the calculated band structures are quite consistent with the ARPES results. The conduction band is very dispersive, indicating that its characters are mostly hybridized 4*d*-5*s* orbitals of Pd, as in the case of $PdCoO_2$. The carrier velocity given by $v_i = \frac{1}{\hbar}\frac{\partial \varepsilon}{\partial k_i}$ at point $P_0$ estimated in the ARPES data is $v_y = 4.9(3)$ eVÅ/$\hbar$, while the velocities at point $P_1$ and $P_2$ in the calculation are 3.4 and 3.3 eVÅ/$\hbar$, respectively. The faster carrier velocity in the ARPES data than that in the band calculation probably originates from the underestimation of the Pd 5*s*-4*d* orbital mixing in the density functional theory by neglecting the correlation effect of Cr 3*d* electrons. The inverse mean free path ($1/l_{MFP} \sim \Delta k = 0.021(1)$ Å$^{-1}$) and the relaxation time ($\tau = 1/v_k\Delta k = 5.7(4) \times 10^{-15}$ s) are comparable to those of $PdCoO_2$.

The electronic structure of the antiferromagnetic phase does not look much different from that of the paramagnetic phase except for the folded bands. Also, the folded bands are almost identical to the original ones at least near the Fermi level as can be compared in Fig. 3c, where they are displayed along the $\Gamma'$-$\Gamma_{AFM}$ line in the antiferromagnetic phase of Fig. 3a top in three different manners, namely the ARPES intensity image (bottom), its waterfall plot derived from the momentum distribution curves near the Fermi level (middle), and the fitted curve at the Fermi level (top), respectively. For example, if we compare the velocity $v_x$ of the folded conduction band at $P_{fold}$ in Fig. 3c to that of $P_{AFM}$ and of $P_{PM}$ in Fig. 3a, all values fall within 4.1(2) eVÅ/$\hbar$. The change of the FS topology in the antiferromagnetic phase can be also readily checked in Fig. 3c. The dispersion of the folded conduction bands (the red dots and the yellow

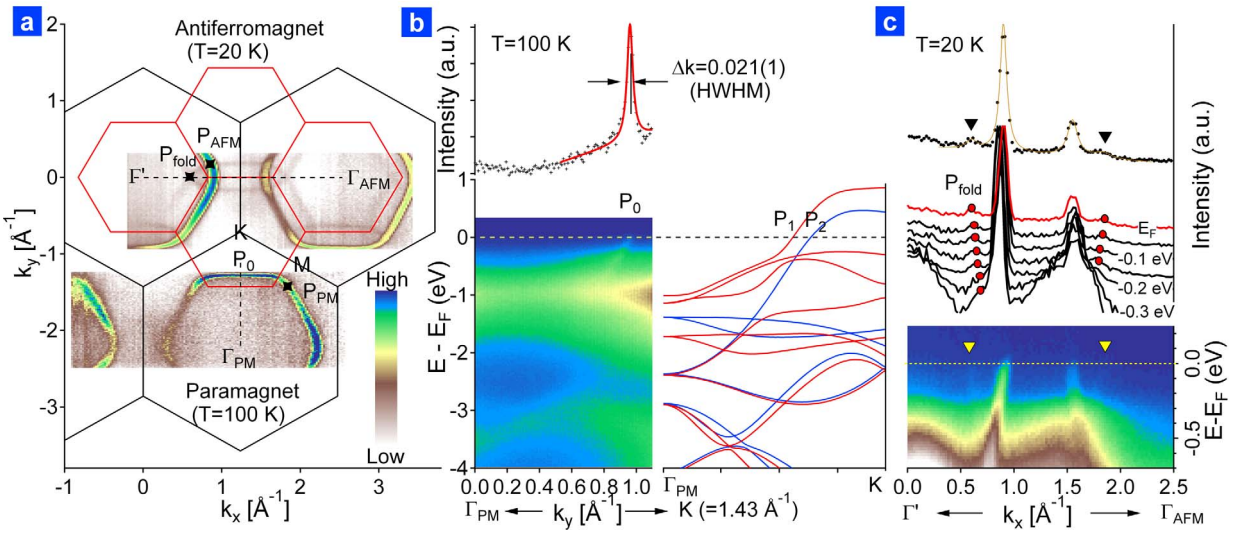


**Figure 3 | Antiferromagnetic transition directly observed by ARPES.** (a), ARPES-measured FSs at the paramagnetic state (lower image) and at the antiferromagnetic state (upper image). The FS foldings corresponding to $\sqrt{3}\times\sqrt{3}\,R30^{\circ}$ superstructure are clearly observed in the antiferromagnetic phase at T = 20 K, while only one hexagonal FS is seen in the paramagnetic phase. The black hexagons are the surface BZs for the (001) surface of the hexagonal crystal unit cell, and the red hexagons are for the magnetic unit cell. (b), ARPES intensity map of paramagnetic $PdCrO_2$ along the Γ-K direction corresponding to the vertical dotted line in (a) (lower left) and the momentum distribution curve at the Fermi level (upper left). The peak width in the momentum distribution curve at the Fermi level measures an inverse mean free path of the conduction electrons. The lower right panel shows the band dispersions along the Γ-K line calculated by the LAPW + LO method. The calculation reproduces most of the major features in the band structure. (c), ARPES intensity map (lower panel), its waterfall plot derived from the momentum distribution curves near the Fermi level (middle panel), and the fitted curve at the Fermi level (upper panel) of antiferromagnetic $PdCrO_2$ along the Γ-K-K-Γ line corresponding to the horizontal dotted line in (a). The folded bands crossing the Fermi level are indicated by the yellow triangles, the red dots, and the black triangles in each panel. In (b) and (c), a reverse color scale is used in comparison with the scale bar in (a).

inverse triangles in each panel) along the $\Gamma'$-$\Gamma_{AFM}$ line produces one hole-like hexagonal FS and two electron-like triangular FSs in a BZ, as shown in Fig. 4.

The detailed analysis on the cross-sectional FS areas in the antiferromagnetic phase is represented in Fig. 4. Based on the ARPES-measured FS image, we determined the size of a rounded hexagonal FS $\delta$ of paramagnetic phase and translated it by the reciprocal lattice vectors to reproduce the folded FSs. The diagonal length and the height in Fig. 4 are 1.94(5) and 1.76(4) $Å^{-1}$, respectively, which are ~5% reduced in comparison with those of $PdCoO_2$. The cross-sectional area of each FS branch is $\alpha$ = 0.083(9), $\beta$ = 0.35(2), $\gamma$ = 1.05(4), and $\delta$ = 2.66(6) $Å^{-2}$, respectively. These are remarkably consistent with the recent quantum oscillation measurements, where the frequency for each FS branch is $\alpha \sim 0.8$, $\beta \sim 3.3$, $\gamma \sim 10.5$, and $\delta \sim 27.5$ kT, respectively[6].

## Discussion

Now that the observed FS folding clearly originates from the localized spin antiferromagnetic ordering, it is important to understand why and how this observation was realized in our ARPES measurements. We think that the key factor is a considerable hybridization between the localized Cr 3*d* orbitals and the itinerant Pd 4*d* orbitals through the oxygen anions. This feature has been also revealed in the recent quantum oscillation study[6]. In the antiferromagnetic phase, in addition to the normal hopping between Pd ions, the conduction electron in the O-Pd-O dumbbells has spin-dependent hopping paths through three kinds of Cr ions A(A'), B(B'), and C(C') in the adjacent upper(lower) layer, as shown in Fig. 1b. Taking into account both the normal hopping and the magnetic hopping, each strength of which is parameterized by $t_0$ and $t_1$ for the magnetic super-cell, we considered a single layer model crystal to set up the tight-binding Hamiltonian described in detail below.

Figure 5 shows the band structure of our model crystal. When the magnetic hopping is absent ($t_0 = 1, t_1 = 0$), the model crystal has one rounded hexagonal FS that resembles the ARPES-measured FS in the paramagnetic phase as shown in Fig. 5a. When turning on the magnetic hopping, the folded bands get their intensities and the antiferromagnetic order of the Cr layers is reflected in the FS map of Fig. 5b

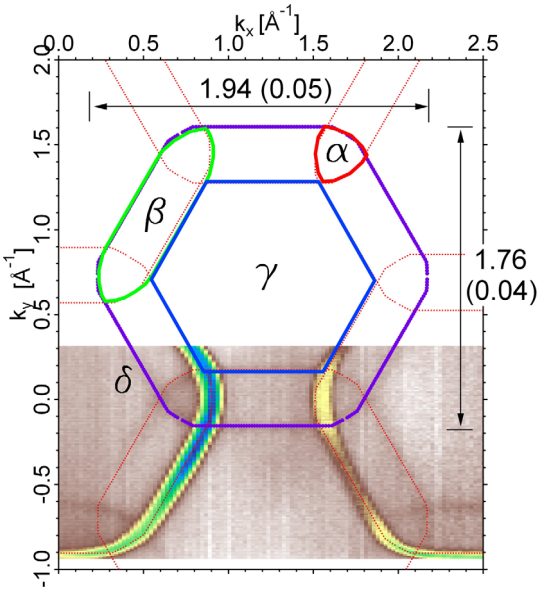


**Figure 4 | Cross-sectional areas of the FSs in the antiferromagnetic phase.** The lower part is the ARPES-measured FSs showing the antiferromagnetic transition. The upper part is the schematic FSs based on the analysis of the cross-sectional areas of the FSs. In the antiferromagnetic phase, there are one hole-like hexagonal FS ($\gamma$) and two electron-like triangular FSs ($\alpha$) in a BZ. Due to the small gap size between the FSs, other shapes of the cross-sectional area, e.g. the lens ($\beta$) and large rounded hexagon ($\delta$), are found. Those were detected by the quantum oscillation measurements[6].

and c. The optimal resemblance is obtained at $t_1 \sim 0.4$ in this model. Here, we point out that the absolute value of $t_1$ can be different from the true value to some degree because of the simplification of our TB model, but it shows a trend consistent with the essential features observed in the ARPES measurements. The success of this model strongly implies that the hybridization between the conduction electrons and the localized spins plays a key role in observing the ordering of the localized spins in ARPES. Actually, this also explains why the surface states observed by Sobota *et al.* do not appear in our ARPES data[20]. The surface states appear in the ARPES data obtained with $\hbar\omega = 55$ eV photons, but are absent in our $\hbar\omega = 120$ eV ARPES data. The photoionization cross section ratio of Cr 3*d* to Pd 4*d* is $\sigma_{(Cr,3d^3)}/\sigma_{(Pd,4d^9)} \sim 0.22$ for 55 eV photons and $\sigma_{(Cr,3d^3)}/\sigma_{(Pd,4d^9)} \sim 6.7$ for 120 eV photons, respectively[21]. Thus, the surface states with mostly Pd 4*d* characters appear much intensely in the 55 eV ARPES data. By the same argument, the folded bands in the antiferromagnetic phase are strongly hybridized with the Cr 3*d* orbitals, so they appear only in our 120 eV ARPES data.

The FS folding due to the antiferromagnetic superstructure observed in ARPES provides a strong constraint on the microscopic origin of the UAHE recently reported in this system. Until now, two studies have reported the UAHE, but the details are quite diverse yet[6,7]. Takatsu *et al.* found an unusual nonlinear field dependence of the Hall resistivity curve, $\rho_{xy}(H)$, with a hump under a magnetic field of 1–3 T at temperatures below $T^* \sim 20$ K, and interpreted it as an UAHE. In order to explain the nonlinearity of $\rho_{xy}(H)$ in the frame of the scalar spin chirality mechanism[22,23], they proposed another magnetic structure with a broken $\sqrt{3} \times \sqrt{3}$ periodicity below $T^*$. Meanwhile, Ok *et al.* measured the Hall resistivity up to $H = 32$ T, and found nonlinearity both at $H \sim 2$ T, $T \lesssim 20$ K and $H \gtrsim 20$ T near the Néel temperature $T_N$. The latter was interpreted as an UAHE possibly originating from the finite scalar spin chirality induced by an external high magnetic field at the temperature region with antiferromagnetic spin-fluctuations, but the former as a magnetic breakdown effect. Our ARPES measurements directly evidenced that the $\sqrt{3} \times \sqrt{3}$ periodicity is sustained at least down to $T = 20$ K. Here, it is worth addressing that the ARPES data was obtained over the whole momentum space, so that the confidence on the new ordering pattern is incomparable to that from other data measured at single momentum point such as diffraction patterns. Combined our ARPES result with the absence of any abrupt behavior in the magnetization curve $M(H)$ as a function of applied magnetic field for $PdCrO_2$[7], the UAHE at the high magnetic field region near $T_N$ is more consistent.

The successful observation of the local spin order by ARPES also suggests a novel method for magnetic structure study of a small two-dimensional crystal such as $AgNiO_2$, $Ag_2MO_2$ (M = Cr, Mn, Ni), $Fe_{1.3}Sb$ or an epitaxial thin film with localized magnetic moments for which neutron scattering is usually not applicable due to the low efficiency. Our experimental results demonstrate that ARPES can be more suitable for these cases if a few metallic layers are covered on the surface with balanced hybridization to the local magnetic moments.

## Methods

The single crystals of $PdCrO_2$ were grown by the NaCl flux method using powder samples described in the literature[24]. The powder samples were synthesized by the following metathetical reaction: $Pd + PdCl_2 + 2LiCrO_2 \rightarrow 2PdCrO_2 + 2LiCl$. In this step, the precursor $LiCrO_2$ was prepared by the solid state reaction method, starting from the stoichiometric mixture of $Li_2CO_3$ and $Cr_2O_3$ at 850°C for 24 hours. The obtained crystals are silvery hexagonal plates, and the typical size is 1.5 × 1.5 × 0.1 $mm^3$. The XRD/ND experiments were performed on the powder samples to check the crystallographic/magnetic phases. The XRD patterns were obtained at the 3A beamline of the Pohang Light Source (PLS) with $\hbar\omega = 11.07$ keV. The ND patterns were obtained at the high-resolution powder-diffraction neutron beamline of HANARO research reactor, Korea. The neutron beam was monochromatized to 1.833 Å by using single-crystal Ge (331) plane.

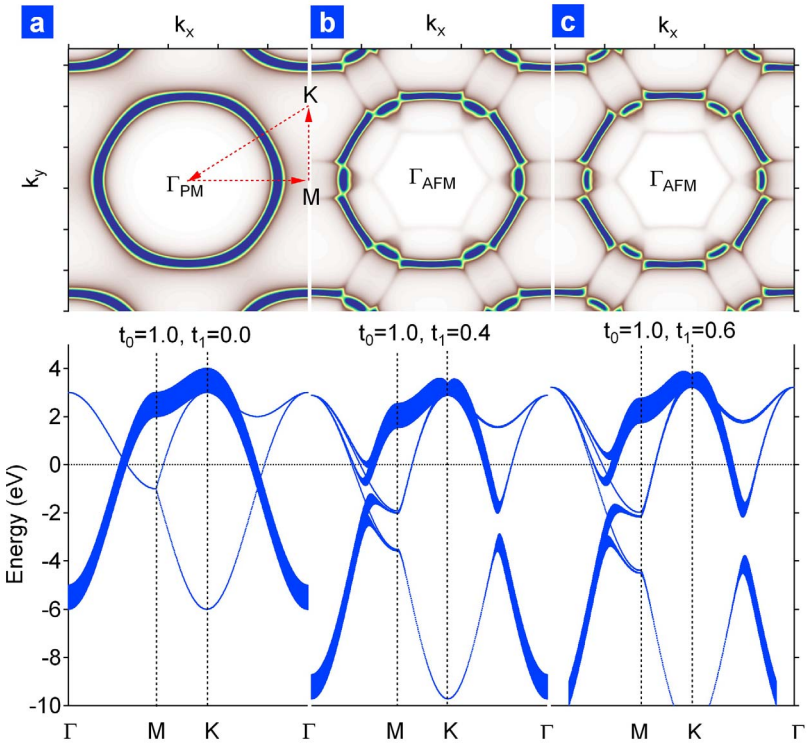


**Figure 5 | Tight-binding calculation results with the minimal model Hamiltonian.** Calculated FS intensity map (upper panel) and the corresponding band dispersions (lower panel) along the Γ-M-K-Γ path (red arrows) of (a) $t_1 = 0.0$ (paramagnetic phase), (b) $t_1 = 0.4$, and (c) $t_1 = 0.6$ ($t_0$ and $t_1$: normal and magnetic hopping strength). In the dispersion curves, the line thickness is proportional to the relative spectral intensity of the eigenstates at a crystal momentum **k**. In the panel (a), the thick line corresponds to an intensity 1, while the thin line to 0. At every momentum point, the sum of all spectral intensities is normalized to 1.

The XAS measurements were performed at the 2A beamline of the PLS. The chamber pressure, resolving power of the photon beam, and the sample temperature were kept at $\sim 10^{-9}$ Torr, 2500, and below 20 K, respectively. After the single crystalline samples were cleaved *in situ*, the absorption spectra were recorded in the total electron yield mode and were normalized by the photon flux.

The photoemission experiments were performed at the 4A1 beamline of the PLS with a Scienta SES-2002 electron spectrometer[25]. Linearly polarized light was incident on the samples with polarization vector parallel to the $k_x$-direction in the ARPES data. The photon energy was set to $\hbar\omega = 120$ eV for ARPES, and to $\hbar\omega = 700$ eV for XPS. The total energy resolution is $\sim$60 meV, and the momentum resolution was set to be $\sim$0.01 $\text{Å}^{-1}$. The crystals were cleaved *in situ* by the top post method at the temperature of 100 K under the pressure of $\sim 7.0 \times 10^{-11}$ Torr. Due to the quasi two-dimensional structure of the crystals, the cleaved surface was shiny and well oriented. After cleaving the samples, we collected the ARPES data in the paramagnetic phase at 100 K, and then lowered the sample temperature to 20 K for the antiferromagnetic measurements. After collecting the low temperature ARPES data in a full range of $k$-space, we raised the sample temperature to 100 K again to check the disappearance of the folded band in a partial range of $k$-space. Unlike the $PdCoO_2$ case[9], we did not apply the thermal cycling process to $PdCrO_2$ since the surface states reported in Ref. 20 were not observed in our ARPES measurements with $\hbar\omega = 120$ eV photon energy.

**Tight-binding model hamiltonian.** As in the case of the $PdCoO_2$ band structure, the bands near Fermi level mainly consist of non-magnetic Pd $4d_{z^2}$ and Pd 5 $s$ hybridized orbitals[10,12]. The Cr moments order as 120° $\sqrt{3} \times \sqrt{3}$ super cell making six Cr spin-dependent hopping paths (see Fig. 1b), but the total moments of Cr around a given O-Pd-O dumbell sum up to zero. Therefore, the magnetic moment of the Pd layer is constraint to zero by symmetry. Here, we ignored all the higher order hopping to make the situation simple, and only consider non-magnetic hopping term $t_0$ (>0), and magnetic hopping term $t_1$ (>0) in our tight-binding Hamiltonian,

$$H = -t_0 \sum_{\langle i,j\rangle\sigma} a^{\dagger}_{j\sigma} a_{i\sigma} - t_1 \sum_{\langle i,j\rangle\sigma\sigma'} a^{\dagger}_{j\sigma} T_{j\sigma,i\sigma'} a_{i\sigma'} = h.c., \quad (1)$$

where $a_i \left(a_i^{\dagger}\right)$ is the annihilation(creation) operator for a conduction electron, and $i$, $j$, $\sigma$, $\sigma'$ are the indices for lattice sites and spin directions, respectively. The magnetic hopping matrix is determined by the direction of Cr moments (overlap of electronic states) in the hopping path, as in the super-exchange. In this calculation, $T_{i\sigma,j\sigma'} = \sum_k \langle i\sigma|S_k\rangle\langle S_k|j\sigma'\rangle$ has been used, where $S_k$ is the Cr moment in the hopping path $k$.

To extract information of band unfolding spectral intensities, we use the following formalism[26]:

$$A_n(k,w) = \sum_{KJ} |<kn|KJ>|^2 \delta(\omega - \epsilon_{KJ}), \quad (2)$$

where $K(k)$ and $J(n)$ denote the super-cell (normal cell) crystal momentum and the band index, respectively. The effect of super-cell potential can be projected to the original BZ, giving spectral intensities. In the tight binding form, the evaluation of $|\langle kn|KJ\rangle|^2$ is trivial, i.e. they are just delta functions which can be determined by spatial relations. To set the Fermi surface, we integrate the states over BZ, and set the number of electron as 1 (half filled) to describe one hole in Pd nominally.


1. Damascelli, A., Hussain, Z. & Shen, Z.-X. Angle-resolved photoemission studies of the cuprate superconductors. *Rev. Mod. Phys.* **75**, 473 (2003).
2. Schäfer, J. *et al.* Direct Spectroscopic Observation of the Energy Gap Formation in the Spin Density Wave Phase Transition at the Cr(110) Surface. *Phys. Rev. Lett.* **83**, 2069 (1999).
3. He, C. *et al.* Electronic-Structure-Driven Magnetic and Structure Transitions in Superconducting NaFeAs Single Crystals Measured by Angle-Resolved Photoemission Spectroscopy. *Phys. Rev. Lett.* **105**, 117002 (2010).
4. Mekata, M. *et al.* Magnetic structure of antiferromagnetic $PdCrO_2$ possible degenerate helices on a rhombohedral lattice. *Physica B* **213&214**, 221 (1995).
5. Takatsu, H. *et al.* Critical behavior of the metallic triangular-lattice Heisenberg antiferromagnet $PdCrO_2$. *Phys. Rev. B* **79**, 104424 (2009).
6. Ok, J. M. *et al.* Quantum oscillations of a metallic triangular-lattice antiferromagnet, $PdCrO_2$. *Phys. Rev. Lett.* **111**, 176405 (2013).
7. Takatsu, H. *et al.* Unconventional Anomalous Hall Effect in the Metallic Triangular-Lattice Magnet $PdCrO_2$. *Phys. Rev. Lett.* **105**, 137201 (2010).
8. Rogers, D. B. *et al.* Chemistry of Noble Metal Oxides. III. Electrical Transport Properties and Crystal Chemistry of $ABO_2$ Compounds with the Delafossite Structure. *Inorg. Chem.* **10**, 723 (1970).
9. Noh, H.-J. *et al.* Anisotropic Electric Conductivity of Delafossite $PdCoO_2$ Studied by Angle-Resolved Photoemission Spectroscopy. *Phys. Rev. Lett.* **102**, 256404 (2009).
10. Noh, H.-J. *et al.* Orbital character of the conduction band of delafossite $PdCoO_2$ studied by polarization-dependent soft x-ray absorption spectroscopy. *Phys. Rev. B* **80**, 073104 (2009).
11. Eyert, V. *et al.* On the Metallic Conductivity of the Delafossites $PdCoO_2$ and $PtCoO_2$. *Chem. Mater.* **20**, 2370 (2008).
12. Kim, K., Choi, H. C. & Min, B. I. Fermi surface and surface electronic structure of delafossite $PdCoO_2$. *Phys. Rev. B* **80**, 035116 (2009).
13. Ong, K. P., Singh, D. J. & Wu, P. Unusual Transport and Strongly Anisotropic Thermopower in $PtCoO_2$ and $PdCoO_2$. *Phys. Rev. Lett.* **104**, 176601 (2010).
14. Anderson, P. W. Resonating valence bonds: A new kind of insulator? *Mater. Res. Bull.* **8**, 153 (1973).
15. Fazekas, P. & Anderson, P. W. On the ground state properties of the anisotropic triangular antiferromagnet. *Philos, Mag.* **30**, 423 (1974).
16. de Groot, F. M. F. *et al.* 2*p* x-ray absorption of 3*d* transition-metal compounds: An atomic multiplet description including the crystal field. *Phys. Rev. B* **42**, 5459 (1990).
17. Dedkov, Y. S. *et al.* Correlations in the electronic structure of half-metallic ferromagnetic $CrO_2$ films: An x-ray absorption and resonant photoemission spectroscopy study. *Phys. Rev. B* **72**, 060401(R) (2005).
18. Doniach, S. & Sunjic, M. Many-electron singularity in X-ray photoemission and X-ray line spectra from metals. *J. Phys. C* **3**, 285 (1970).
19. Wertheim, G. K. & Hüfner, S. Many-Body Line Shape in X-Ray Photoemission from Metals. *Phys. Rev. Lett.* **35**, 53 (1975).
20. Sobota, J. A. *et al.* Electronic structure of the metallic antiferromagnet $PdCrO_2$ measured by angle-resolved photoemission spectroscopy. *Phys. Rev. B* **88**, 125109 (2013).
21. Yeh, J. J. & Lindau, I. Atomic Data and Nuclear Data Tables. **32**, 1–155 (1985).
22. Nagaosa, N. *et al.* Anomalous Hall effect. *Rev. Mod. Phys.* **82**, 1539 (2010).
23. Xiao, D., Chang, M.-C. & Niu, Q. Berry phase effects on electronic properties. *Rev. Mod. Phys.* **82**, 1959 (2010).
24. Takatsu, H. & Maeno, Y. Single crystal growth of the metallic triangular-lattice antiferromagnet $PdCrO_2$. *J. Cryst. Growth.* **312**, 3461 (2010).
25. Kim, H.-D. *et al.* Performance of a Micro-Spot High-Resolution Photoemission Beamline at PAL. *AIP conf. Proc.* **879**, 477 (2007).
26. Ku, W., Berlijn, T. & Lee, C.-C. Unfolding First-Principles Band Structures. *Phys. Rev. Lett.* **104**, 216401 (2010).


## Acknowledgments

This work was supported by the National Research Foundation (NRF) of Korea Grant funded by the Korean Government (MEST) (Nos. 2010-0010771 and 2012M2B2A4029607). K.K. and B.I.M. acknowledge the support of NRF (Nos. 2009-0079947 and 2011-0025237) and KISTI (No. KSC-2012-C2-27). H.D.K. was supported by NRF funded by MEST (No. 2009-0090561).

## Author contributions

The whole research was planned by H.J.N. $PdCrO_2$ crystals were grown by J.J. ARPES measurements were performed by H.J.N., J.J., D.J., H.S.M., E.J.C., B.G.P. and H.D.K. Transport measurements were performed by J.J. and J.S.K. XAS measurements were performed by H.J.N., J.J., H.K.L. and J.Y.K. ND/XRD experiments were performed by J.J., B.C., S.L., J.M.O. and B.G.P. TB calculations were done by K.K. and B.I.M. J.Y.K. and H.K.L. maintained the XAS endstation. H.D.K. and B.G.P. maintained the ARPES endstation. H.J.N. wrote the paper with suggestions and comments by J.S.K., K.K., B.I.M. and H.D.K.

## Additional information

**Competing financial interests:** The authors declare no competing financial interests.

**How to cite this article:** Noh, H.-J. *et al.* Direct Observation of Localized Spin Antiferromagnetic Transition in $PdCrO_2$ by Angle-Resolved Photoemission Spectroscopy. *Sci. Rep.* **4**, 3680; DOI:10.1038/srep03680 (2014).